Contents lists available at ScienceDirect

Chemical Engineering Research and Design

journal homepage: www.elsevier.com/locate/cherd

Experimental and theoretical study of the thermal decomposition of ethyl acetate during fast pyrolysis

Diana C. Vargas[a,b], *Sebastián Salazar*[a], *José R. Mora*[a], *Kevin M. Van Geem*[b], *Daniela Almeida Streitwieser*[a,*]

[a] *Universidad San Francisco de Quito USFQ, Department for Chemical Engineering, Institute for Development of Alternative Energies and Materials IDEMA, Diego de Robles s/n, 170901 Quito, Ecuador*

[b] *Ghent University, Laboratory for Chemical Technology, Center for Sustainable Chemistry (CSC), Technologiepark 125, 9052 Gent, Belgium*

ARTICLE INFO

Article history:
Received 11 October 2019
Received in revised form 26 February 2020
Accepted 1 March 2020
Available online 7 March 2020

Keywords:
Pyrolysis
Ethyl acetate
Thermal decomposition
Unimolecular decomposition
Arrhenius equation
Activation energy

ABSTRACT

The thermal decomposition of ethyl acetate was experimentally studied in a newly designed fast pyrolysis set-up. The results were compared to theoretical calculations and literature values in order to proof the experimental concept. The reaction was carried out in a free fall tubular reactor with a residence time of 0.15 s. The identification and quantification of products stream composition was performed online using a GC-TCD/FID. First, an overview of the reaction rate at feed volumes of 0.25, 0.50 and 0.75 mL was obtained at reaction temperature between 400 to 600 °C in intervals of 50 °C. As a result mass transfer limitation for feeds larger than 0.5 mL were identified. For the second approach, a constant feed volume of 0.25 mL and temperatures between 420 to 550 °C were investigated. Using the experimental results, a global kinetic model is proposed for the thermal decomposition of ethyl acetate into ethylene and acetic acid through a first order unimolecular reaction. Also, theoretical calculations were performed at ωB97XD/6-311++G(d,p) level. A concerted mechanism through a six-membered transition state was identified in the reaction path. The theoretical and experimental activation energy values lie within the literature values between 193 and 213 kJ/mol.

1. Introduction

The use of fossil fuels have a negative impact on the environment due to CO_2 emissions, which are increasing in the atmosphere affecting the climate conditions (Atabani et al., 2012). Also, due to the limited reserves of non-renewable energy sources, the energy sustainability cannot be guaranteed for fossil fuels in the near future (Kothari et al., 2010; Zhang et al., 2016). These factors motivate the development of new technologies for the production of fuels, chemicals and alternative materials from renewable raw materials. Liquid biofuels are already being used as a replacement for petroleum-based fuels (Atabani et al., 2012; Wang et al., 2019). In the U.S., Europe and other countries, ethanol and biodiesel are blended with gasoline and diesel fuels, or are used as fuels on their own (Zhang et al., 2016; Anon, 2018; Baeyens et al., 2015). The utilization of ethanol or biodiesel implies that less gasoline and diesel fuels are being burnt, which reduces the requirements of crude oil and mitigates the atmospheric contamination resulting in less net CO_2 emissions to the atmosphere (Anon, 2018).

Fast pyrolysis is a thermochemical technology in which compounds with large carbon containing molecules, like hydrocarbons or carbohydrates, are shortened by adding heat in absence of oxygen (Bridgwater, 2012; Choi et al., 2018). The products from pyrolysis are obtained in liquid, gaseous and solid phase, known as bio-oil, pyrolysis gas and biochar, respectively (Kung and Zhang, 2015). The advantages of pyrolysis

* *Corresponding author.*
E-mail addresses: dalmeida@usfq.edu.ec, danialmeidastr@gmail.com (D. Almeida Streitwieser).
https://doi.org/10.1016/j.cherd.2020.03.001

are its high thermal efficiency and low CO_2, SO_x and NO_x emissions (Apaydin-Varol et al., 2014; Preciado-Hernandez et al., 2019). Moreover, fast pyrolysis of biomass is one of the most promising routes for the production of alternative energies and green chemical precursors (Stefanidis et al., 2014). In the case of fast pyrolysis, thanks to the short residence time in the range of seconds or below, the main product is the bio-oil with yields between 40% to 75% (Akhtar and Saidina Amin, 2012). The composition of the bio-oil depends on the feedstock, experimental parameters and collection technique (Sharifzadeh et al., 2019). This liquid contains high quantities of water (15–50 wt%), coming from the moisture of the feedstock as well as from the pyrolysis reactions. Since the main interest on fast pyrolysis of biomass lies in the potential conversion into liquid bio-fuels or green chemicals (Zhang et al., 2016), which can be stored or transported easily (Azargohar et al., 2013), the removal of the water content is imperative. The bio-oil contains also large amounts of oxygenated compounds which can cause corrosion to the motor and other parts when uses as a fuel (Wang et al., 2019; Van De et al., 2010). An upgrade can be achieved through the following processes: hydrodeoxygenation, catalytic vapor cracking—in situ or ex situ and gasification to syngas followed by synthesis to hydrocarbons or alcohols (Sharifzadeh et al., 2019).

Biomass is defined as all the organic matter that is available on a renewable basis, including industrial waste products from agriculture and forestry (Almeida Streitwieser, 2017; Van de Velden et al., 2010). Biomass can be used as renewable source for pyrolysis, since it does not contribute to the increase of CO_2 emissions (Lu et al., 2009). Although biomass pyrolysis proceeds through a complex network of reactions, the study of its reaction mechanism can be simplified by using model molecules with similar molecular structures in such a way that the biomass reactions are mimicked. The model molecule used for this investigation is ethyl acetate, that is an alkyl ester, containing C—O, CO, CC, and CH——— bonds, which can be representative of some of the more important bonds found in part of the biomass, and which is well known that decomposes thermally mainly to acetic acid and ethylene (AlAbbad et al., 2017; Metcalfe et al., 2007; Martín and Chuchani, 1981; Saheb and Hosseini, 2013; Tosta et al., 2010; Adejoro and Bamkole, 2009) (Fig. 1).

The thermal decomposition of ethyl acetate follows a first order unimolecular reaction (Silva, 2007). The accepted mechanism involves an unimolecular six-centered transition state producing equimolar ethylene and acetic acid (Metcalfe et al., 2007; Silva, 2007; Ren et al., 2014; Kuo et al., 2014), where the polarization of the C—O bond is reported as the determining factor in the rate limiting step (Ren et al., 2014). In the present work, ethyl acetate was chosen as a model molecule for the determination of a kinetic model of its thermal decomposition by using

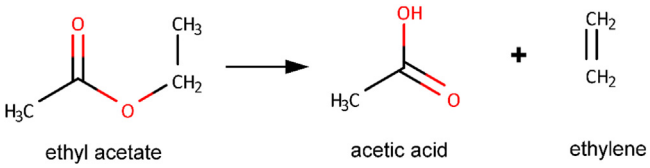

Fig. 1 – Thermal decomposition of ethyl acetate.

a new designed fast pyrolysis set-up. The kinetic and thermodynamic parameters are obtained experimentally by applying the Arrhenius and Eyring equation at a temperature range from 400 to 600 °C. The results are compared to the theoretical kinetic and thermodynamic properties which are calculated at the level of theory ωB97XD/6-311++G(d,p). Finally, the experimental activation energy obtained from the Arrhenius equation is compared with the theoretical value obtained from the calculations with Gaussian 09, as well as with other reported values from literature.

2. Materials and methods

2.1. *Experimental set-up*

The unimolecular decomposition of ethyl acetate was studied in a ceramic tubular pyrolysis reactor with an inner diameter of 2.5 cm and a reaction section of 45 cm wrapped in a heating jacket Carbolite Gero model VST 12/300. Helium was used as the carrier gas with a flow rate of 50 mL/s with a temperature controller Eurotherm 3508. Ethyl acetate was injected with a syringe through the feeding system on the top of the tubular reactor (Fig. 1). The thermal decomposition reaction takes place and a fraction of the products stream at the bottom of the reactor goes directly to the gas chromatograph by a stainless steel pipelines system, which analyzes the sample on line. The remaining gas stream is purged to eliminate the overpressure in the reactor. The flow diagram for the fast pyrolysis set-up for liquid injection is shown in Fig. 2.

2.2. *Temperature measurements*

Before starting the experimental investigation, a temperature profile for the reactor was obtained to define the isothermal zone in the reaction zone. The thermocouple used for this

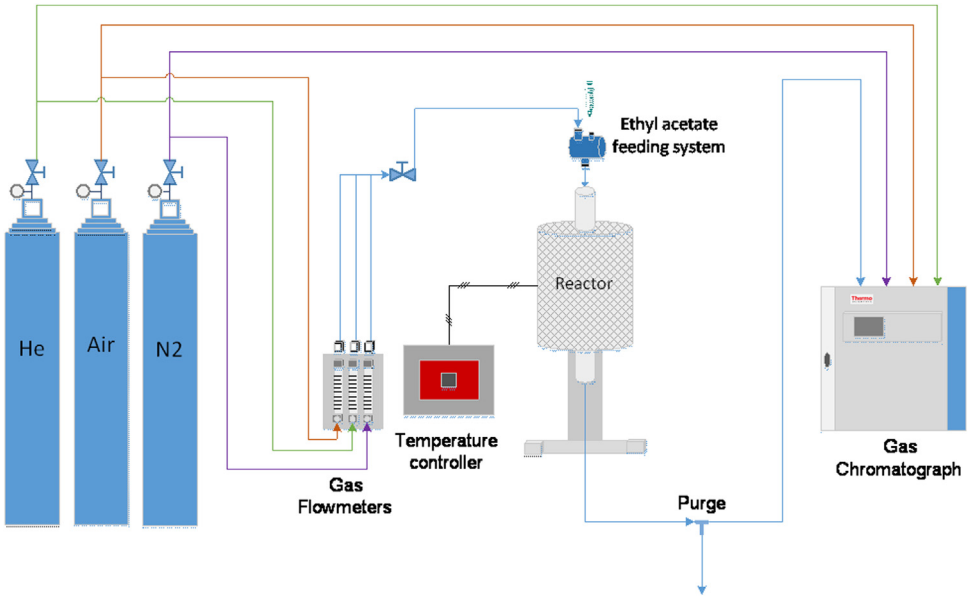

Fig. 2 – Flow diagram for pyrolysis set-up for liquid injection.

Table 1 – Experimental conditions parameter screening and kinetic analysis.

Parameter	Units	Initial screening	Kinetic analysis
Reactor temperature	[°C]	400–600	420–550
Temperature steps	[°C]	50	10
Reactor pressure	[bar]	0.829	0.829
Sample residence time	[s]	0.15	0.15
Reactant gas rate	[mL/s]	50	50
Sample feed	[mL]	0.25 / 0.5 / 0.75	0.25

measurements is a single 3/16̈diameter Inconel Type K Thermocouple with a length of 800 mm. The temperature profile for the reactor is shown in Fig. 2. The temperature measurements show an isothermal zone in the heated zone of the reactor of 30 cm. Thus the assumptions of isothermal system are confirmed for the different reaction temperatures.

2.3. Design of experiments

The experimental conditions are presented in Table 1 for initial screening and for the kinetic analysis. The goal is to obtain the kinetic parameters for the thermal decomposition of ethyl acetate. Therefore, temperature and sample feed were varied, while the flow rate was kept constant to maintain a constant residence time in all experiments. Therefore, temperature and sample feed were varied, while the flow rate at normal conditions was kept constant. The residence time of ethyl acetate in the reaction zone was calculated by adding the linear velocity given by the flow rate at real conditions and the gravity force acting during free fall on the reactant, resulting in a constant residence time of 0.15 s.

2.4. Reactants

Ethyl acetate was bought from Fischer Scientific, purity grade: 99.5%. Acetic acid (glacial), 100% anhydrous for analysis, was also supplied by Fischer Scientific. Mixture of standard gases (Scott Mini-mix) was supplied by Air Liquid with a composition of methane 1%, ethane 1%, acetylene 1%, carbon dioxide 1%, carbon monoxide 1%, and ethylene 1% in nitrogen. The carrier gases helium with UHP grade 5.0 and nitrogen UHP grade 5.0 were supplied by Linde.

2.5. Analytical methodology

The products from the pyrolysis of ethyl acetate were analyzed by a gas chromatograph (GC) Thermo Scientific model Trace 1310 with a split/splittless injector and a GSV (gas sampling valve). The column used is a TG Bond Q Thermo Scientific 15 m × 0.53 mm × 20 μm with a nonpolar, 100% divinyl benzene phase. The GC is coupled with both flame ionization detector (FID) and thermal conductivity detector (TCD) for characterization and quantification. The thermal decomposition of ethyl acetate was analyzed with both detectors. The injections of the products stream sample were made online through a gas sampling valve (GSV). The oven temperature program started at 30 °C, hold for 5 min and heated at a rate of 10 °C/min–220 °C. The column flow rate was 2.1 mL/min, split flow 60.1 mL/min and the sampling time 0.4–0.75 min. The specification of the analytical conditions in the GC can be found in the supplementary information SM1.

External calibration was used to identify and quantify ethyl acetate, acetic acid and ethylene fractions. For acetic acid and ethyl acetate different volumes of the pure compounds were injected into the GC, while for ethylene the standard gas mixture of gases described in Section 2.3 was used. These compounds were injected in the feeding system with a constant helium stream while using the same analytical conditions in the gas chromatograph. The reactor was kept at a low temperature (200 °C) to prevent any decomposition of the compounds. The retention time in the column for the three compounds of interest are shown in the supplementary information.

2.6. Kinetics analysis

According to previous investigations reported in literature, various reaction pathways for the unimolecular reaction of ethyl acetate may occur. These pathways are summarized in Table 2 (Metcalfe et al., 2007; Martín and Chuchani, 1981; Saheb and Hosseini, 2013; Tosta et al., 2010). Even though all of the reaction pathways proposed could have contributions to the overall reaction, the majority of experimental studies have mainly focused on mechanism 1, which has proven to be the dominant reaction pathway (Martín and Chuchani, 1981; Saheb and Hosseini, 2013; Tosta et al., 2010) and the products obtained in this work (acetic acid and ethylene) confirm this statement. For this study the first mechanism based on an elimination pathway proposed by Martín and Chuchani, (1981), Saheb and Hosseini, (2013) and Tosta et al. (2010) will be used for developing the equations of the reactor design presented next (Mora et al., 2008; Lezama et al., 2009; Brea et al., 2012; Marquez et al., 2010).

Based on the reactor design, the vertical tube can be considered an isothermal plug flow reactor (PFR) at stationary state during the course of the reaction. The mass diagram for the reactor is shown in Fig. 3. The rate of change, R_A, expressed as the rate of consumption of A (ethyl acetate) can be obtained experimentally with the mass balance of the PFR presented in Eq. (1).

$$F_A|_Z - F_A|_{z+dz} + R_A dV = 0 \quad (1)$$

Where F_A is the molar flow rate of the reactant A in L/s, entering the control space at z and exiting at z + dz. R_A is the rate of consumption of A in mol/L·s and is defined as the sum of the individual reaction rates, r_A, multiplied by its stoichiometric coefficients, ν_A, $R_A = \sum \nu_A (r_A)$. And dV is the differential volume element, Adz.

As mentioned before, in this study the decomposition reaction of ethyl acetate is considered as a first order elemental reaction according to Eq. (2).

$$CH_3COOC_2H_5 \rightarrow CH_2 = CH_2 + CH3COOH \quad (2)$$

$$A \rightarrow B + C$$

Thus, the rate of consumption of A can be expressed as presented in Eq. (3).

$$R_A = -r_A = -kC_A \quad (3)$$

The molar flow rate, F_A, and the concentration, C_A, can be expressed in terms of the conversion, X_A. An expansion factor, ε_A, of 2 should be considered in the expression given in concentrations, if a pure reactant would be introduced in the gas

Table 2 – Reaction mechanisms proposed for ethyl acetate.

Mechanism	Reaction	Source
1	$CH_3COOC_2H_5 \rightarrow CH_2=CH_2+CH_3COOH$	Metcalfe et al. (2007); Martín and Chuchani (1981); Saheb and Hosseini (2013); Tosta et al. (2010)
2	$CH_3COOC_2H_5 \rightarrow 2CH_3COH$	Adejoro and Bamkole (2009)
3	$CH_3COOC_2H_5 \rightarrow CH_3CH_2OH+CH_2CO$	Saheb and Hosseini (2013)
4	$CH_3COOC_2H_5 \rightarrow CH_3COO\cdot + \cdot C_2H_5$	Saheb and Hosseini (2013)
	$CH_3COOC_2H_5 \rightarrow CH_3COOCH_2\cdot + \cdot CH_3$	
	$CH_3COOC_2H_5 \rightarrow CH_3CO\cdot + \cdot OC_2H_5$	
	$CH_3COOC_2H_5 \rightarrow CH_3COOCH\cdot CH_3 + \cdot H$	
	$CH_3COOC_2H_5 \rightarrow H\cdot + \cdot CH_2COOC_2H_5$	
	$CH_3COOC_2H_5 \rightarrow CH_3COOC_2H_4\cdot + \cdot H$	

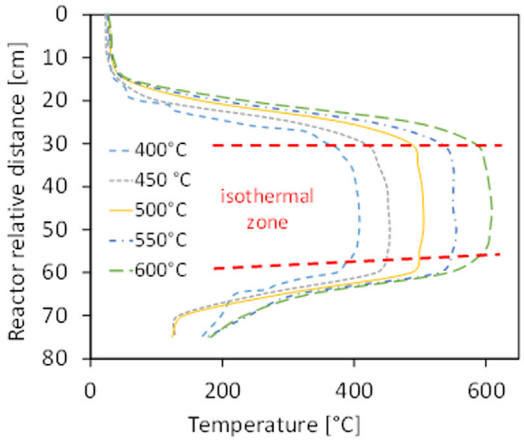

Set Temperature [°C]	Measured Temperature [°C]
400	401.6 ± 7.0
450	446.1 ± 8.6
500	501.7 ± 3.7
550	549.0 ± 4.5
600	602.7 ± 5.9

Fig. 3 – Temperature profiles for the reactor and definition of the isothermal zone for each experimental conditions.

phase reaction. But since inert gas helium in a ratio of 4000:1 is introduced, an expansion factor of zero can be expected and a process with constant density can be assumed. By rearranging Eq. (1) in terms of the differential volume, Eq. (4) is obtained.

$$-\frac{dF_A}{dz}dz = -R_A dV = r_A A dz$$

$$dV = -\frac{F_{A0}dX_A}{kC_{A0}(1-X_A)} \tag{4}$$

Combining and rearranging the terms in the previous equations, an expression for the volume variation dV is obtained. By integrating between 0 and V for the volume and from 0 to X_A for the conversion of ethyl acetate, Eq. (5) is obtained. Where τ is the residence time, defined as the reaction volume over the volumetric flow rate. For the feeding volume of 0.25 mL, the temperature was varied between 420 to 550 °C keeping a constant residence time of 0.15 s.

$$\int_0^V dV = -\int_0^{X_A} \frac{C_{A0}\dot{V}dX_A}{kC_{A0}(1-X_A)}$$

$$k = -\frac{1}{\tau}\ln(1-X_A) \tag{5}$$

The experimental activation energy can be found by plotting the linearized Arrhenius equation, ln (k) vs 1/T, as is shown in Eq. (6). For each set of experiments, activation energy and pre-exponential factor were determined. To obtain the graphics ln (k) vs 1/T, the kinetic constant was calculated with the conversion as previously shown in Eq. (5). The slope of the linearized equation is equal to (- E_a/R), and the pre-exponential factor is obtained from the antilogarithm of the intersection value with the y-axis.

$$lnk = lnk_0 - \frac{Ea}{RT} \tag{6}$$

2.7. Computational methodology

The program Gaussian 09 (Frisch et al., 2016) was used to calculate the theoretical activation energy for the thermal decomposition of ethyl acetate (AlAbbad et al., 2017) As a first stage of the study, the molecules of the reactant and the transition state (TS) were drawn in Gauss View 5.0. With the resulting models, a scan of the geometry of ethyl acetate molecule was performed to obtain the structure with the minimum global energy. Upon obtaining the equilibrium geometry for the reactant, a further optimization and vibrational analysis was conducted. All DFT calculations were performed using the ωB97XD/6-311++G(d, p) level (Villegas-Escobar et al., 2017). This functional uses a version of Grimme's D2 empirical dispersion (Adejoro and Bamkole, 2009; Ren et al., 2014). ωB97XD functional has previously shown to estimate the transition states geometries more accurately for hydrogen abstraction and radical recombination reactions as compared to other computationally expensive levels of theory (Stefan, 2006). The thermodynamic properties were determined using the vibrational analysis obtained previously for each stationary point (reactant and transition state). In the particular case of the TS structure, the presence of only one imaginary frequency was evidenced. Intrinsic reaction coordinate calculations were used in order to associate the TS to the ethyl acetate (reactant) and the two products (ethylene and acetic acid) (Saheb and Hosseini, 2013). The absolute enthalpies obtained for the ethyl acetate and the TS allow to determine the enthalpy of

activation (Eq. 7) (McQuarrie and Simon, 1997). The activation enthalpy can be calculated with the electronic energy and an enthalpy correction term as shown in Eq. (8) (McQuarrie and Simon, 1997). An estimation of the theoretical activation energy was calculated with Eq. (9).

$$H^{\ddagger} = H_{TS} - H_{react} \tag{7}$$

$$H^{\ddagger} = (\varepsilon_0 + H_{corr})_{TS} - (\varepsilon_0 + H_{corr})_{react} \tag{8}$$

$$E_a = \Delta H^{\ddagger} + RT \tag{9}$$

Where $\Delta H^{\ddagger}$ corresponds to the activation enthalpy of the reaction path, $(\varepsilon_0)_{TS}$ is the total electronic energy of transition state, $(H_{corr})_{TS}$ is the correction to the enthalpy due to internal energy of transition state, $(\varepsilon_0)_{react}$ corresponds to the total electronic energy of reactant, $(H_{corr})_{react}$ is the correction to the enthalpy due to internal energy of reactant, E_a is the activation energy, R is the ideal gas constant and T is the system's temperature.

The Eyring-Polanyi formulation (Evans and Polanyi, 1935) of the rate constant correlates the rate constant with the activation free energy of the system as expressed in Eq. (10).

$$k = \frac{k_B T}{h} e^{-\Delta G^{\ddagger}/RT} \tag{10}$$

Where k_B is the Boltzmann constant (1.381×10^{-23} J/K), h is Planck's constant (6.626×10^{-34} Js), T is the temperature in K, and $\Delta G^{\ddagger}$ is the activation free energy of the system expressed in J/mol.

Combining the Eyring-Polanyi formulation and the Arrhenius equation, the correlation from Eq. (11) is obtained to calculate the pre-exponential factor, k_0, using the thermodynamics values obtained from Gaussian 09 software.

$$\log k_0 = \log\left(\frac{k_B T}{h} e^1\right) + \frac{\Delta S^{\ddagger}}{2.303R} \tag{11}$$

The Arrhenius equation was used for each set of experiments and a non-linear adjustment was made to determine the parameter that fit the Arrhenius equation at each injected volume.

3. Results and discussion

3.1. Experimental results

During the first approach, the experiments for the thermal decomposition of ethyl acetate were performed at different temperatures for the feed volumes 0.25, 0.50 and 0.75 mL.

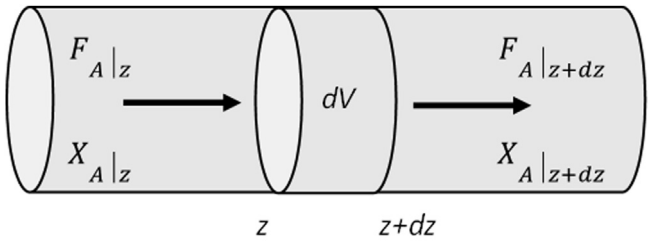

$$F_A\big|_Z - F_A\big|_{z+dz} + R_A dV = 0$$

Fig. 4 – Mass diagram for a PFR.

The chromatograms presented in Supplemental Information (SM2 and SM3) show the peaks in the FID detector of the unreacted ethyl acetate and the products: acetic acid and ethylene at different reaction temperatures. The intensity of the peaks can be compared to the different temperatures for each feed volume. As expected, at the higher pyrolysis temperature the peak of ethyl acetate decreases, while the peaks for acetic acid and ethylene increase. The pyrolysis temperatures were selected based on the literature available, which states that below 400 °C no appreciable decomposition of the ethyl acetate was observed (Martín and Chuchani, 1981; Saheb and Hosseini, 2013; Mai et al., 2017).

At 400 °C no peaks of ethylene and acetic acid can be observed in the chromatograms (Figure SM3), showing that the conversion of ethyl acetate is nearly zero. At 450 °C the chromatograms show a minimum conversion, and as the reaction temperature increases to 500 °C and 550 °C, the productsṕeaks can be clearly identified. Finally, at 600 °C, the ethyl acetate peak is insignificant compared to the product peaks of ethylene and acetic acid. This is most evident with the smallest feed volume of ethyl acetate, where the peak almost disappears. Using external calibration with the previously described standards, the peaks of the different compounds were converted to concentration. The decomposition of ethyl acetate, as well as the formation of the products, are represented in terms of weight percentages and for the kinetic analysis, it is expressed as the conversion of A, X_A, as shown in Fig. 5 (a).

In Fig. 5 (a) the curve for ethyl acetate conversion, X_A, as function of reaction temperature can be observed. The curves show different trends for the three feeding volumes. While for the experiments using 0.25 and 0.50 mL feeding volumes the curves show an 'S'-shaped behavior, for 0.75 mL feed the conversion obtained shows a linear dependency with temperature. This indicates that the short residence time of 0.15 s may not be enough to thermally decompose completely the

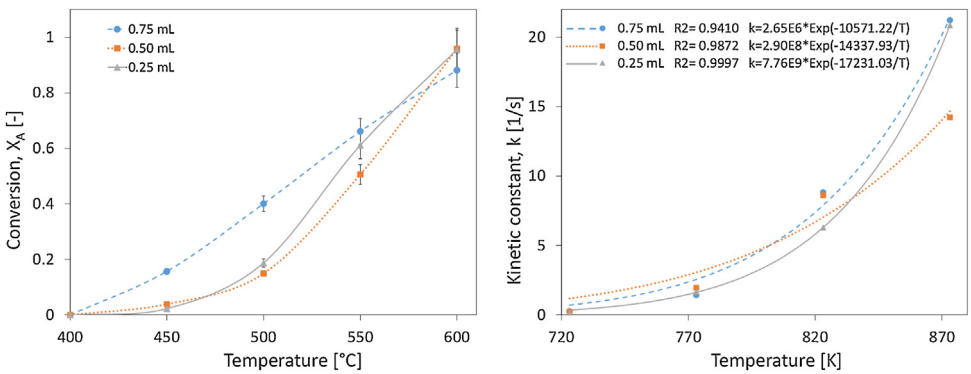

Fig. 5 – (a) Conversion of ethyl acetate (b) Non-linear adjustment for the Arrhenius equation at 0.25, 0.50 and 0.75 mL.

Table 3 – Experimental and theoretical kinetic parameters.

Study	Ea [kJ/mol]	Log ko [-]	Temperature range [°C]	Residence time [min]	Type of study
Experimental results	198.47	13.93	420–550	1.8×10^{-3}	Tubular reactor Helium as inert gas
Simulation results	205.97	13.91	500	–	Theoretical simulation
Adejoro and Bamkole, 2009	203.51	12.45	350	–	Theoretical simulation
Blades (1954)	199.79	12.48	350	2.5×10^{-3}	Experimental, quartz reactor with Toluene atmosphere
Blades and Gilderson, 1960	200.83	12.59	350	1.3×10^{-2}	Experimental, quartz reactor with Toluene atmosphere
Saheb and Hosseini (2013)	213.93	13.61	560	–	Theoretical simulation
Tosta et al. (2010)	200.4	12.55	400	–	Theoretical simulation

injected ethyl acetate due to lack in heat supply during the reaction (Van De et al., 2010; Marquez et al., 2010; Van de Velden et al., 2008). Later in this study, mass and heat transfer limitations within the reactor will be calculated. Fig. 4 (b) shows the adjustment to the non-linearized Arrhenius equation for the three different feeding volume experiments. The correlation coefficients for the feeding volumes of 0.75 and 0.50 mL are 0.9410 and 0.9872, respectively, while a good correlation was observed for 0.25 mL with a correlation coefficient of 0.9997.

This suggests that at high feeding volumes of ethyl acetate the rate of decomposition of the reactant is being limited by mass and heat transfer processes, caused by its high concentration and short residence times. This can also be observed by the lower activation energy values obtained for the higher feeding volumes in Table 3, which can be explained by the influence of the low diffusion coefficients observed in mass transfer processes. This observation suggests that heat and mass transfer limitations play an important role in the rate of decomposition, the degree of conversion and the product formation at feeding volumes of 0.5 mL or higher.

In order to understand if the short residence time allow a complete heat and mass transfer between the liquid reactant and the helium stream, or whether heat and mass transfer limitations must be considered, a selection of dimensionless numbers are calculated to correlate mass and energy transfer phenomena (Krishna and Standart, 1979), such as Reynolds, Schmidt, Prandtl, Lewis, Peclet, Nusselt and Sherwood numbers.

The value obtained for the Reynolds number of 1342 is smaller than 2100 which means that the fluid follows a laminar regime, thus indicating an inefficient momentum transfer. The Schmidt and Prandtl numbers are based on material properties, temperature and pressure, and not dependent on the flow of the system. The Prandtl number correlates the relation between the momentum diffusivity and the thermal diffusivity of the fluid. In this case the fluid is helium and a very small Prandtl number of 0.103 indicates that heat diffuses very fast compared to momentum. The Schmidt number with a value of 1.26×10^{-5}, on the other hand, correlates momentum diffusivity with mass diffusivity, and in this case it indicates that mass diffusivity is slow compared to momentum. The relationship between Schmidt and Prandtl is given by Lewis number, the obtained value is 12.03, a value >1 indicates a higher thermal to mass diffusion ratio, indicating that mass transfer is the limiting step in this set-up.

Also the Peclet number is small (0.017), indicating that diffusive mass transport is more important than convective mass transport, confirming the assumption that mass diffusion is the limiting step, especially in the cases with higher feed volume of 0.5 and 0.75 mL.

The Nusselt and Sherwood numbers represent the effectiveness of heat and mass convection at the surface. The Nusselt number represents the ratio between heat transfer by convection and conduction of a fluid. The value obtained in this system is 8.026 which is larger than 1 showing that heat transfer occurs mainly by convection. Heat conduction is, thereafter, enhanced by the forced motion of the fluid. On the other hand, the small value obtained for the Sherwood number, the dimensionless mass transfer coefficient, of 5.9×10^{-6}, confirms a limitation of mass transfer by diffusion.

3.2. *Kinetics investigation*

Based on the results of the initial parameter screening and the analysis of the heat and mass transfer limitation with dimensionless numbers, only a feeding volume of 0.25 mL is used for the kinetic investigation. Each experiment is repeated three times for replicability and the temperature is varied in steps of 10 °C as described in Table 1. The exit gas stream is analyzed again by GC-FID and the areas of the chromatograms are converted to concentration of the reactants and products by calibrating the peeks with the standards as described in Section 3.1. In Fig. 6 (a), the weight percentages for the reactant and the two products are presented as function of the reaction temperature. As observed, the formation of acetic acid and ethylene follow the same trend since the decomposition follow a first order kinetic reaction and their formation have a stoichiometric relationship. In Fig. 6 (b), the calculated degree of conversion of the ethyl acetate as function of the reaction temperature is presented. The 'S'-shaped curve shows that at temperatures below 480 °C the ethyl acetate does not undergo decomposition. The conversions starts to be significant at 500 °C when it reaches almost 20%, while at 550C the conversion reaches 50% and, finally, at 600 °C it ranges around 95%. The uncertainty for each measurement is also shown in Fig. 6. The lowest value is ±2% and reaches up to 5%. The uncertainty increases as the conversion of ethyl acetate reaches 100% since the unreacted ethyl acetate approaches the detection limits.

Using the linearized Arrhenius (Eq. 9) for the experiments with a feeding volume of 0.25 mL, the experimental value for the activation energy is found to be 198.47 kJ/mol and for the pre-exponential factor a value of 8.49E + 13 s^{-1} is found as depicted in Fig. 6.

3.3. *Computational calculations*

Complementary to the experimental study, the optimized 3D structure at ωB97XD/6−311 G(d,p) level for the reactant (ethyl acetate) and the transition state are shown in Fig. 7. Vibrational frequencies were calculated at the same level of theory and all minima were ensured to have zero imaginary frequen-

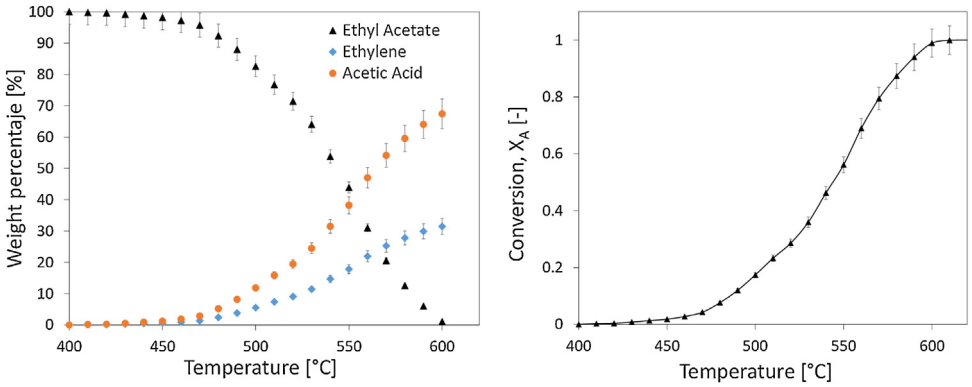

Fig. 6 – (a) Weight percentages of ethyl acetate and its decomposition products (b) Ethyl acetate conversion as a temperature function.

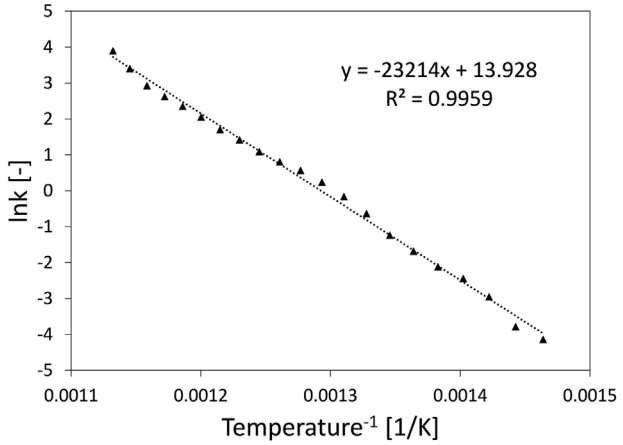

Fig. 7 – Linearized Arrhenius equation for 0.25 mL feed.

cies. This computational study includes the thermochemical parameters, energies and geometries of reactant, transition state and products.

The theoretical activation energy of ethyl acetate thermal decomposition, E_a, was calculated for each experimental temperature. The values of the activation energy, E_a, do not change with temperature as expected. The values for the calculated E_a in a range of temperatures from 400 to 600 °C vary between 205.04 and 206.83 kJ/mol with a standard deviation of 0.705 kJ/mol. The theoretical activation energy value of 205.97 kJ/mol obtained at 500 °C was used for the comparison to the experimental activation energy. The exact values for the temperature range are presented in Table SM4. (Fig. 8)

These results are supported by the values of activation energy as well as the logarithmic form of the pre-exponential factor for the decomposition of ethyl acetate reported in literature as presented in Table 3. The systems studied in literature were batch reactions with residence times from 0.15 to 1800 seconds (Saheb and Hosseini, 2013; Tosta et al., 2010; Adejoro and Bamkole, 2009; Blades, 1954; Blades and Gilderson, 1960) compared to the residence time of 0.15 s in the falling plug flow reactor of this study. Nonetheless, the reported activation energy values in literature vary between 193.00 and 213.93 kJ/mol (Tosta et al., 2010; Adejoro and Bamkole, 2009), showing that the theoretical as well as the experimental values presented in this work lie within the same range. By comparing the activation energy values obtained from the experimental data and the theoretical calculations with the parameters from literature as shown in Table 3, a variation of 5 kJ/mol can be observed while the pre – exponential factor varies between the literature, the experimental data and the simulation in one order of magnitude. The pre – exponential factor gives information about the system used, the size of the ring of the transition state and the bond polarization in the rate limiting state (Sabbe et al., 2010).

4. Conclusions

In this work, the pyrolysis of ethyl acetate was investigated as a model molecule in a new designed fast pyrolysis setup. The first experimental approach allowed to determine the favorable conditions range for the determination of the kinetic parameters and to identify mass transfer limitations at higher feeding volumes. Therefore, in the second experimental approach only the smallest feeding volume of 0.25 mL was investigated, to obtain more significant experimental data for the kinetic evaluation. It was assumed that the reaction followed a first order unimolecular decomposition mechanism, following the observation that the only products formed between 400 °C and 650 °C were ethylene and acetic acid. Using the experimental results from the kinetic

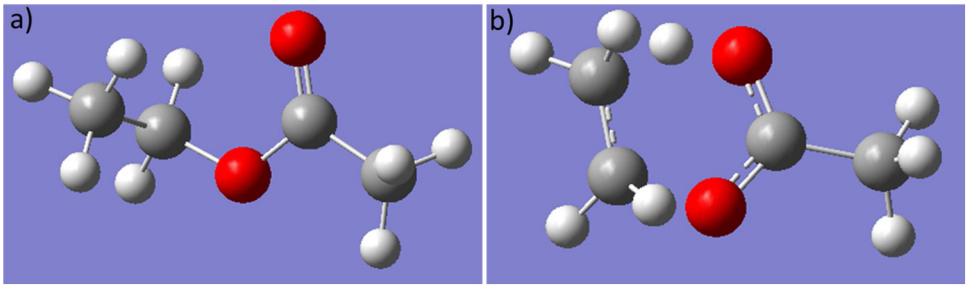

Fig. 8 – (a) Optimized structure of ethyl acetate molecule. (b) Optimized transition state for ethyl acetate molecule thermal decomposition.

approach a value of 198.47 kJ/mol for the activation energy was obtained, while the theoretical value calculated with Gaussian was 205.97 kJ/mol. These values are in good agreement with those in the literature that vary between 199 and 213 kJ/mol.

This investigation is a key step in studying the thermal decomposition of more complex molecules or natural compounds, where a C—O bond decompose by polarization is expected as in this case. Some molecules that will have a similar decomposition pathway that are of interest in the future are monolignols with phenolic radicals and will be investigated in next studies.

Conflict of interest

Authors confirm that there wasn't any conflict of interest.

Acknowledgments

This research has been supported by the Belgian Development Cooperation through VLIR-UOS. VLIR-UOS supports partnerships between universities and university colleges, in Flanders and in the South. The study has also been supported by the USFQ Collaboration Grant 2017.

References

Adejoro, I.A., Bamkole, T.O., 2009. Kinetics and mechanism of elimination of ethyl acetate in the gas phase: a theoretical study. African J. Pure. Appl. Chem. 3 (8), 140–144.

Akhtar, J., Saidina Amin, N., 2012. A review on operating parameters for optimum liquid oil yield in biomass pyrolysis. Renewable Sustainable Energy Rev. 16 (7), 5101–5109, http://dx.doi.org/10.1016/j.rser.2012.05.033.

AlAbbad, M., Giri, B.R., Szőri, M., Farooq, A., 2017. On the high-temperature unimolecular decomposition of ethyl levulinate. Proc. Combust. Inst. 36 (1), 187–193, http://dx.doi.org/10.1016/j.proci.2016.06.034.

Almeida Streitwieser, D., 2017. Comparison of the anaerobic digestion at the mesophilic and thermophilic temperature regime of organic wastes from the agribusiness. Bioresour. Technol. 241, 985–992, http://dx.doi.org/10.1016/j.biortech.2017.06.006.

Anon, 2018. U.S. Energy Information Administration. Biofuels: Ethanol & Biodiesel, Published https://www.eia.gov/energyexplained/index.php?page=biofuel_home.

Apaydin-Varol, E., Uzun, B.B., Önal, E., Pütün, A.E., 2014. Synthetic fuel production from cottonseed: fast pyrolysis and a TGA/FT-IR/MS study. J. Anal. Appl. Pyrolysis 105, 83–90, http://dx.doi.org/10.1016/j.jaap.2013.10.006.

Atabani, A.E., Silitonga, A.S., Badruddin, I.A., Mahlia, T.M.I., Masjuki, H.H., Mekhilef, S., 2012. A comprehensive review on biodiesel as an alternative energy resource and its characteristics. Renewable Sustainable Energy Rev. 16 (4), 2070–2093, http://dx.doi.org/10.1016/j.rser.2012.01.003.

Azargohar, R., Jacobson, K.L., Powell, E.E., Dalai, A.K., 2013. Evaluation of properties of fast pyrolysis products obtained, from Canadian waste biomass. J. Anal. Appl. Pyrolysis 104, 330–340, http://dx.doi.org/10.1016/j.jaap.2013.06.016.

Baeyens, J., Kang, Q., Appels, L., Dewil, R., Lv, Y., Tan, T., 2015. Challenges and opportunities in improving the production of bio-ethanol. Prog. Energy Combust. Sci. 47, 60–88, http://dx.doi.org/10.1016/j.pecs.2014.10.003.

Blades, A.T., 1954. The kinetics of the pyrolysis of ethyl and isopropyl formates and acetates. Can. J. Chem. 32 (4), 366–372, http://dx.doi.org/10.1139/v54-049.

Blades, A.T., Gilderson, P.W., 1960. The secondary hydrogen isotope effects in the pyrolisis of ethyl- d 5 acetate and ethyl Acetate- d 3. Can. J. Chem. 38 (9), 1407–1411, http://dx.doi.org/10.1139/v60-196.

Brea, O., Loroño, M., Marquez, E., Mora, J.R., Cordova, T., Chuchani, G., 2012. Theoretical study of methoxy group influence in the gas-phase elimination kinetics of methoxyalkyl chlorides. Int. J. Quantum Chem. 112 (12), 2504–2514, http://dx.doi.org/10.1002/qua.23244.

Bridgwater, A.V., 2012. Review of fast pyrolysis of biomass and product upgrading. Biomass Bioenergy 38, 68–94, http://dx.doi.org/10.1016/j.biombioe.2011.01.048.

Choi, Mkyu, Park, H.C., Choi, H.S., 2018. Comprehensive evaluation of various pyrolysis reaction mechanisms for pyrolysis process simulation. Chem. Eng. Process: Process Intensif. 130, 19–35, http://dx.doi.org/10.1016/j.cep.2018.05.011.

Evans, M.G., Polanyi, M., 1935. Some applications of the transition state method to the calculation of reaction velocities, especially in solution. Trans Faraday Soc 31 (12), 875–894, http://dx.doi.org/10.1039/tf9353100875.

Frisch, M.J., Trucks, G.W., Schlegel, H.B., Scuseria, G.E., Robb, M.A., Cheeseman, J.R., Scalmani, G., Barone, V., Petersson, G.A., Nakatsuji, H., Li, X., Caricato, M., Marenich, A., Bloino, J., Janesko, B.G., Gomperts, R., Mennucci, B., 2016. Gaussian 09, Revision A.02, WC. Gaussian 09 Citation.

Kothari, R., Tyagi, V.V., Pathak, A., 2010. Waste-to-energy: a way from renewable energy sources to sustainable development. Renewable Sustainable Energy Rev. 14 (9), 3164–3170, http://dx.doi.org/10.1016/j.rser.2010.05.005.

Krishna, R., Standart, G.L., 1979. Mass and energy transfer in multicomponent systems. Chem. Eng. Commun. 3 (4–5), 201–275, http://dx.doi.org/10.1080/00986447908935865.

Kung, C.C., Zhang, N., 2015. Renewable energy from pyrolysis using crops and agricultural residuals: an economic and environmental evaluation. Energy 90, 1532–1544, http://dx.doi.org/10.1016/j.energy.2015.06.114.

Kuo, W.C., Avedisian, C.T., Choi, K.H., Tsang, W., 2014. On using film boiling to thermally decompose liquid organic chemicals: application to ethyl acetate as a model compound. Int. J. Heat Mass Transf. 68, 456–465, http://dx.doi.org/10.1016/j.ijheatmasstransfer.2013.08.054.

Lezama, J., Márquez, E., Mora, J.R., Córdova, T., Chuchani, G., 2009. Theoretical calculations on the mechanisms of the gas phase elimination kinetics of chlorocyclohexane, 3-chlorocyclohexene and 4-chlorocyclohexene. J. Mol. Struct. THEOCHEM 916 (1–3), 17–22, http://dx.doi.org/10.1016/j.theochem.2009.08.029.

Lu, Q., Li, W.Z., Zhu, X.F., 2009. Overview of fuel properties of biomass fast pyrolysis oils. Energy Convers. Manage. 50 (5), 1376–1383, http://dx.doi.org/10.1016/j.enconman.2009.01.001.

Mai, T.V.T., Duong, Mvan, Nguyen, H.T., Lin, K.C., Huynh, L.K., 2017. Kinetics of thermal unimolecular decomposition of acetic anhydride - an integrated deterministic and stochastic model. J. Phys. Chem. A, http://dx.doi.org/10.1021/acs.jpca.7b00015, acs.jpca.7b00015.

Marquez, E., Domínguez, R.M., Mora, J.R., Córdova, T., Chuchani, G., 2010. Experimental and theoretical studies of the homogeneous, unimolecular gas-phase elimination kinetics of trimethyl orthovalerate and trimethyl orthochloroacetate. J. Phys. Chem. A 114 (12), 4203–4209, http://dx.doi.org/10.1021/jp1005296.

Martín, I., Chuchani, G., 1981. Steric acceleration in the pyrolysis kinetics of 2-substituted ethyl acetates. J. Phys. Chem. 85 (25), 3902–3904, http://dx.doi.org/10.1021/j150625a039.

McQuarrie, D.A., Simon, J.D., 1997. Physical Chemistry: A Molecular Approach. University Science Books, Sausalito.

Metcalfe, W.K., Dooley, S., Curran, H.J., Simmie, J.M., El-Nahas, A.M., Navarro, M.V., 2007. Experimental and modeling study of $C_5H_{10}O_2$ ethyl and methyl esters †. J. Phys. Chem. A 111 (19), 4001–4014, http://dx.doi.org/10.1021/jp067582c.

Mora, J.R., Domínguez, R.M., Herize, A., Tosta, M., Chuchani, G., 2008. Kinetics and mechanisms of gas-phase elimination of 2,2-diethoxyethyl amine and 2,2-diethoxy-N,n-diethylethanamine. J. Phys. Org. Chem. 21 (5), 359–364, http://dx.doi.org/10.1002/poc.1339.

Preciado-Hernandez, J., Zhang, J., Zhu, M., Zhang, Z., Zhang, D., 2019. An experimental study of CO2 gasification kinetics during activation of a spent tyre pyrolysis char. Chem. Eng. Res. Des. 149, 129–137, http://dx.doi.org/10.1016/J.CHERD.2019.07.007.

Ren, W., Mitchell Spearrin, R., Davidson, D.F., Hanson, R.K., 2014. Experimental and modeling study of the thermal decomposition of C3-C5 ethyl esters behind reflected shock waves. J. Phys. Chem. A 118 (10), 1785–1798, http://dx.doi.org/10.1021/jp411766b.

Sabbe, M.K., Reyniers, M.F., Waroquier, M., Marin, G.B., 2010. Hydrogen radical additions to unsaturated hydrocarbons and the reverse β-scission reactions: modeling of activation energies and pre-exponential factors. Chem. Phys. Chem. 11 (1), 195–210, http://dx.doi.org/10.1002/cphc.200900509.

Saheb, V., Hosseini, S.M.A., 2013. Theoretical studies on the kinetics and mechanism of multi-channel gas-phase unimolecular reaction of ethyl acetate. Comput. Theor. Chem. 1009, 43–49, http://dx.doi.org/10.1016/j.comptc.2012.12.030.

Sharifzadeh, M., Sadeqzadeh, M., Guo, M., et al., 2019. The multi-scale challenges of biomass fast pyrolysis and bio-oil upgrading: review of the state of art and future research directions. Prog. Energy Combust. Sci. 71, 1–80, http://dx.doi.org/10.1016/j.pecs.2018.10.006.

Silva, A.M., 2007. A theoretical study of the pyrolysis of isopropyl acetate. Chem. Phys. Lett. 439 (1–3), 8–13, http://dx.doi.org/10.1016/j.cplett.2007.03.037.

Stefan, G., 2006. Semiempirical GGA-type density functional constructed with a long-range dispersion correction. J. Comput. Chem. 27 (15), 1787–1799, http://dx.doi.org/10.1002/jcc.20495.

Stefanidis, S.D., Kalogiannis, K.G., Iliopoulou, E.F., Michailof, C.M., Pilavachi, P.A., Lappas, A.A., 2014. A study of lignocellulosic biomass pyrolysis via the pyrolysis of cellulose, hemicellulose and lignin. J. Anal. Appl. Pyrolysis 105, 143–150, http://dx.doi.org/10.1016/j.jaap.2013.10.013.

Tosta, M.M., Mora, J.R., Cordova, T., Chuchani, G., 2010. Journal of Molecular Structure : THEOCHEM Quantum chemical calculations of the homogeneous, unimolecular, gas-phase elimination kinetics of primary alkyl acetates and (dimethylamino) alkyl acetates : neighboring group participation in 4- (dimethylami. J Mol Struct THEOCHEM 952 (1–3), 46–55, http://dx.doi.org/10.1016/j.theochem.2010.04.017.

Van De, Velden M., Baeyens, J., Brems, A., Janssens, B., Dewil, R., 2010. Fundamentals, kinetics and endothermicity of the biomass pyrolysis reaction. Renew. Energy 35 (1), 232–242, http://dx.doi.org/10.1016/j.renene.2009.04.019.

Van de Velden, M., Baeyens, J., Boukis, I., 2008. Modeling CFB biomass pyrolysis reactors. Biomass Bioenergy 32 (2), 128–139, http://dx.doi.org/10.1016/J.BIOMBIOE.2007.08.001.

Van de Velden, M., Baeyens, J., Brems, A., Janssens, B., Dewil, R., 2010. Fundamentals, kinetics and endothermicity of the biomass pyrolysis reaction. Renew. Energy 35 (1), 232–242, http://dx.doi.org/10.1016/j.renene.2009.04.019.

Villegas-Escobar, N., Toro-Labbé, A., Becerra, M., Real-Enriquez, M., Mora, J.R., Rincon, L., 2017. A DFT study of hydrogen and methane activation by B(C6F5)3/P(t-Bu)3 and Al(C6F5)3/P(t-Bu)3 frustrated Lewis pairs. J. Mol. Model. 23 (8), 234, http://dx.doi.org/10.1007/s00894-017-3404-y.

Wang, M., Dewil, R., Maniatis, K., et al., 2019. Biomass-derived aviation fuels: challenges and perspective. Prog. Energy Combust. Sci. 74, 31–49, http://dx.doi.org/10.1016/j.pecs.2019.04.004.

Zhang, H., Baeyens, J., Cáceres, G., Degrève, J., Lv, Y., 2016. Thermal energy storage: recent developments and practical aspects. Prog. Energy Combust. Sci. 53, 1–40, http://dx.doi.org/10.1016/j.pecs.2015.10.003.